

# Experimental TTT Diagram of HAYNES 282 Alloy



M. G. Fahrmann and L. M. Pike

**Abstract** HAYNES<sup>®</sup> 282<sup>®</sup> alloy was developed by Haynes International as an age-hardenable, yet fabricable, wrought Ni-base superalloy. To date, the alloy has been specified for a number of applications, most notably in the hot sections of both aero- and industrial gas turbines. A Time-Temperature-Transformation (TTT) diagram is a useful guide to assess an alloy's behavior during thermo-mechanical processing and heat treating. Starting with the (commercially relevant) 1149 °C (2100 °F) mill-annealed condition, a time (0.1–100 h)—temperature (649–1121 °C (1200–2050 °F)) exposure matrix was executed. Precipitates, which had formed as a result of these exposures, were analyzed by light microscopy, scanning electron microscopy/energy dispersive spectroscopy (SEM/EDS), and, in selected cases, by x-ray diffraction (XRD). Chiefly,  $\gamma'$  and two types of carbides, Cr-rich  $M_{23}C_6$  and Mo-rich  $M_6C$ , were found. Approximate C-curves for these phases were constructed, and some implications for the alloy's processing and properties characteristics are discussed.

**Keywords** 282 alloy · TTT diagram · Gamma-Prime · Carbides

## Introduction

HAYNES<sup>®</sup> 282<sup>®</sup> alloy was developed by Haynes International [1] as a wrought, high-creep-strength, yet fabricable alternative to alloys such as Waspaloy. To date, the alloy has been specified for a number of applications, most notably in the hot gas path sections of both aero- and industrial gas turbines.

---

M. G. Fahrmann (✉) · L. M. Pike  
Research and Technology Department, Haynes International Inc.,  
Kokomo, IN, USA  
e-mail: mfahrmann@haynesintl.com

L. M. Pike  
e-mail: lpike@haynesintl.com

In order to understand and control the alloy's behavior during thermo-mechanical processing (e.g., rolling, forging) and heat treating (solution-annealing and aging), an experimental TTT diagram is a useful guide. No such diagram has heretofore been generated for this alloy. We stress the emphasis on experimental since, in principle, TTT diagrams can nowadays also be constructed by means of computational thermodynamics and kinetics [2–4]. However, the latter approach still requires the input of crucial experimental parameters, such as interfacial energies for meaningful predictions.

The presented work follows a rather practical approach: we chose the mill-annealed condition for a starting point rather than trying to create a hypothetical, single-phase initial condition. In fact, the latter is virtually impossible to achieve in the presence of strong carbide and nitride formers such as titanium. This means that certain constituents, notably primary carbides/nitrides, would already be present prior to thermal exposure. We also note that the construction of the C-curve for a secondary phase would ideally refer to a certain specified volume fraction of this phase. Such detailed quantitative measurements were beyond the scope of this study; instead, we focus on the practical aspects of the observed transformations. For example, we address the implications of these constituents for strength and ductility.

## Material and Experimental Methods

The nominal composition of 282 alloy is shown in Table 1. The material of this study originated from commercially produced 1.6 mm (0.062") thick sheet stock that was mill-annealed at 1149 °C (2100 °F). This particular product form was selected since it represents one of the most chemically homogeneous states on account of its thermo-mechanical processing history. In addition, lab heat treatments of sheet coupons result in rapid thermal equilibration, thus minimizing uncertainty, particularly for short exposure times.

The time-temperature exposure matrix covered times of 0.1, 1, 10, and 100 h and temperatures of 649 (1200), 704 (1300), 760 (1400), 816 (1500), 871 (1600), 927 (1700), 982 (1800), 1038 (1900), 1093 (2000), and 1121 °C (2050 °F). This matrix was, in part, devised based on the known age-hardening characteristics of the alloy [5]. Temperature in the laboratory box furnace used was controlled to better than  $\pm 5.6$  °C (10 °F).

The thermally exposed sheet coupons were cut in half; one half was used for hardness readings on the Rockwell A scale, the other half was used for

**Table 1** Nominal composition of HAYNES 282 alloy (in wt%)

Ni	Co	Fe	Cr	Mo	Mn	Si	Al	Ti	C	B
Bal.	10	1.5 <sup>a</sup>	20	8.5	0.3 <sup>a</sup>	0.15 <sup>a</sup>	1.5	2.1	0.06	0.005

<sup>a</sup>Maximum

metallographic preparation employing standard metallographic techniques. Two different electrolytic etching techniques were employed to reveal various phases: (a) “ $\gamma'$  etch” using a mixture of 15 g  $\text{CrO}_3$  + 150 ml  $\text{H}_3\text{PO}_4$  + 10 ml  $\text{H}_2\text{SO}_4$ , and (b) “carbide-etch” using 5 g oxalic acid dissolved in 95 ml HCl.

SEM/EDS work was performed on a ZEISS SIGMA FEG SEM equipped with a SDD detector. Secondary, back-scattered, and high-resolution in-lens imaging modes were employed. The standard-less EDS work was typically done at 10 kV (thus minimizing the beam-sample interaction volume), utilizing the L peaks for the heavier elements.

Phase extraction/XRD work was performed on a limited basis, chiefly for 100-h exposures only. The extraction solution used was 5% HCl + 5%  $\text{H}_3\text{PO}_4$ , balance being methanol. The extracted powders were analyzed in a PANalytical X'Pert<sup>3</sup> powder diffractometer using  $\text{CuK}\alpha$  radiation. The  $2\theta$  scan range was approximately  $20^\circ$ – $90^\circ$  at a scan rate of  $0.020^\circ$  per step and a dwell time 1 s per step. The diffraction peaks were indexed using the current database of the International Centre for Diffraction Data [6]. Only the evidence of phases for which multiple strong diffraction peaks were found, was considered conclusive.

Particle size analysis of  $\gamma'$  encompassed manual tracing of a sufficient number of particles ( $N > 100$ ) on multiple high-magnification, high-resolution SEM in-lens micrographs. The traced images were subsequently digitized and processed using the public-domain image processing software Image J [7]. Since these samples were deep-etched, no correction for particle truncation was deemed necessary. Also, since only particles with well-defined perimeters (no overlaps) were traced, no volume fraction measurements were attempted. In order to assess the impact of bias in the tracing procedure, selected sets of micrographs were traced independently by two different persons, and then processed and analyzed to the same protocol.

## Results and Discussion

### *Initial Condition*

A representative photomicrograph of the initial (mill-annealed) condition is shown in Fig. 1. The average grain size was rated as ASTM 3. The presence of scattered particle stringers in the rolling direction is not uncommon to superalloy sheet products. Notice that the grain boundaries exhibit only a very light, if any decoration. More detail about these particle stringers is shown in the BSE micrograph in Fig. 2. SEM/EDS analyses indicate that three different types of particles, subsequently referred to as primary carbides, are present in the mill-annealed sheet stock:

- (a) TiN nitrides, often in a core-rim configuration with the rim presumably being a carbide,
- (b) Ti- and Mo-rich MC-type carbides,
- (c) Mo-rich  $\text{M}_6\text{C}$ -type carbides.

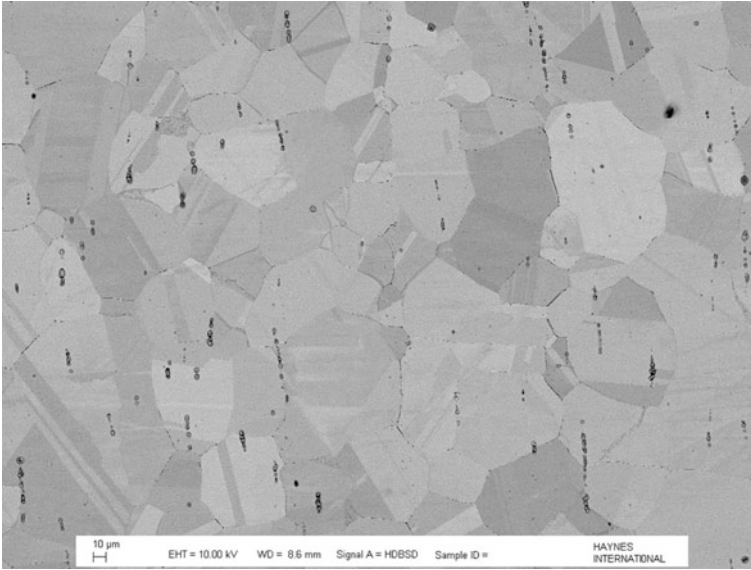


**Fig. 1** SEM BSE photomicrograph of the 282 alloy sheet samples in the initial, mill-annealed condition exhibiting stringers of primary carbides

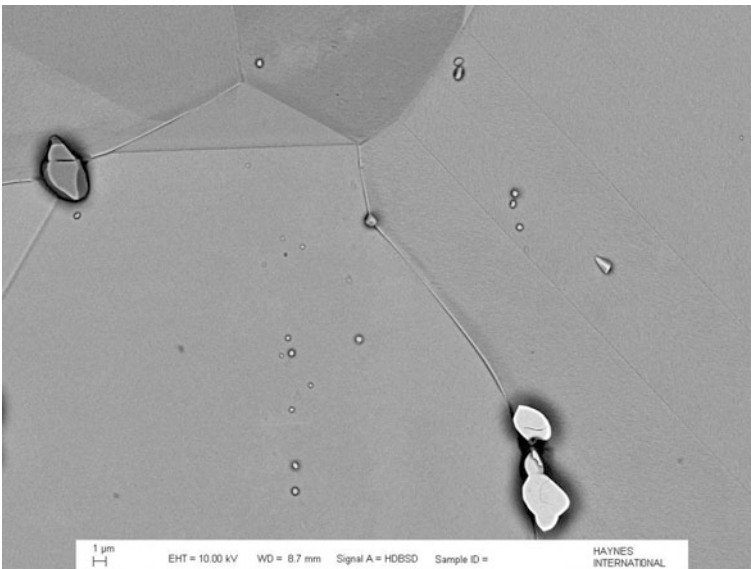


**Fig. 2** High-magnification SEM BSE photomicrograph of the 282 alloy sheet samples in the initial, mill-annealed condition exhibiting primary MC (dark) and primary M<sub>6</sub>C (bright) carbides



**Fig. 3** Very high magnification SEM in-lens photomicrograph of the 282 alloy sheet samples in the initial, mill-annealed condition indicating the presence of very fine cooling  $\gamma'$

The TiN particles formed presumably during melting and served subsequently as nucleation sites for carbides during solidification. The MC-type and the  $M_6C$ -type carbides are believed to be solidification products. The combination of size, morphology, location, and stringer-like arrangement of these primary carbides served as a crucial footprint for their distinction from any secondary carbides that formed upon thermal exposure.

While not detectable on traditional LM micrographs, high-magnification in-lens imaging in the SEM revealed the presence of what appears to be cooling  $\gamma'$  (Fig. 3). These very small, densely packed features tended to be spherical in shape and of a diameter of roughly 10 nm. The presence of cooling  $\gamma'$  in this alloy is to be expected; on a mill-scale, its precipitation cannot realistically be suppressed [8]. Nonetheless, hardness is low (roughly 90 HRB) and ductility/formability is high (tensile elongation in excess of 50%) in this condition.

### ***Thermal Exposures—Gamma-Prime***

Since  $\gamma'$  appeared to be already present in the initial condition, a classical C-curve could not be generated for this phase. Taking the aforementioned rather practical approach, the evolution of average  $\gamma'$  size during aging was tracked instead. Measuring average  $\gamma'$  size was meaningful since these particles tended to be

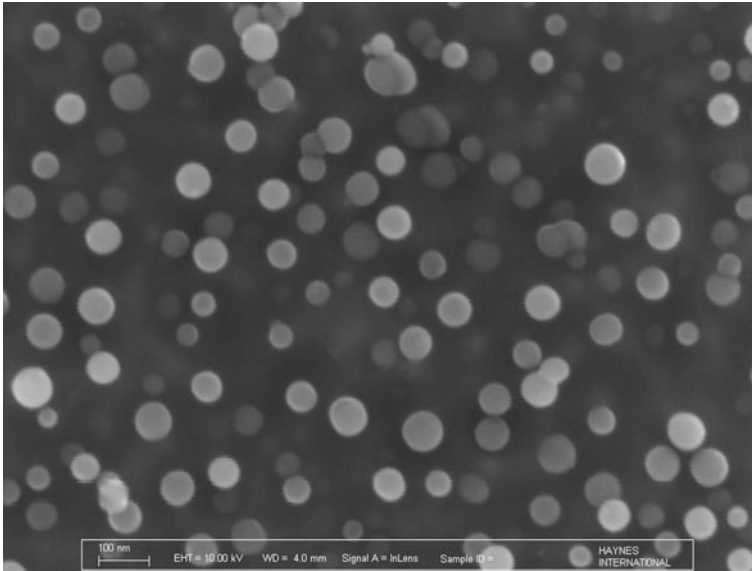


**Fig. 4** High-magnification SEM in-lens photomicrograph of a 282 alloy sheet sample exposed at 927 °C (1700 °F) for 1 h, exhibiting spheroidal intragranular  $\gamma'$

spherical in shape and mono-modal in size distribution for all thermal exposures. An example substantiating this claim is provided in Fig. 4.

The average  $\gamma'$  diameter as a function of aging time is plotted in Fig. 5, aging temperature being the curve parameter. Notice that 982 °C (1800 °F) is the upper limit in this plot since no  $\gamma'$  was detected after aging at 1038 °C (1900 °F), consistent with a  $\gamma'$  solvus temperature of approximately 1000 °C (1830 °F) [5]. The uncertainty in the average diameters is estimated to be on the order of the symbol size, based on the aforementioned independent measurements by two persons. This plot is useful since it allows one to correlate heat treat parameters with the size of the resulting strengthening  $\gamma'$  precipitates. For example, based on the generated Time-Temperature-Hardness (TTH) diagram in Fig. 6 (notice the Rockwell A scale), the optimal aging condition (maximum hardness in minimum time) appears to be 788 °C (1450 °F)/8 h, as recommended for the alloy [5]. Further discussion of the recommended heat treatment for 282 alloy will follow later in this manuscript. Referencing Fig. 6, the corresponding mean  $\gamma'$  diameter after 788 °C (1450 °F)/8 h would be roughly 30 nm. Conversely, one could estimate the magnitude of the age-hardening effect (and infer its impact on processability) if the material is held at any of these studied temperatures during manufacturing. We note that the temperature-dependent  $\gamma'$  volume fraction needs to be factored in such estimates as well.

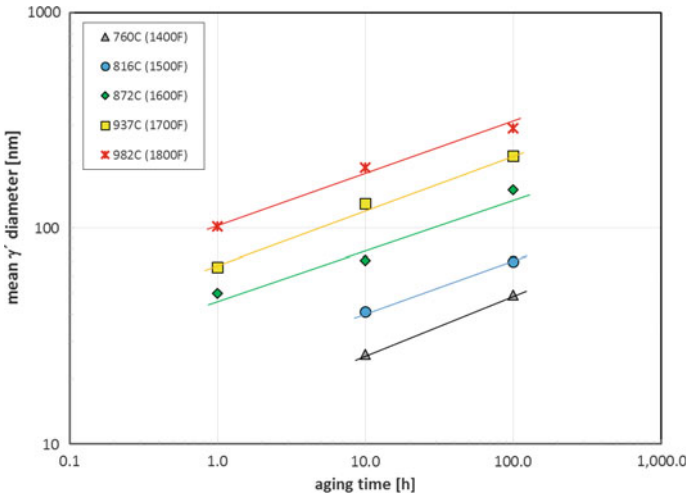


Fig. 5 Plot of the measured mean intragranular  $\gamma'$  diameter in the 282 alloy sheet samples as a function of the thermal exposure conditions

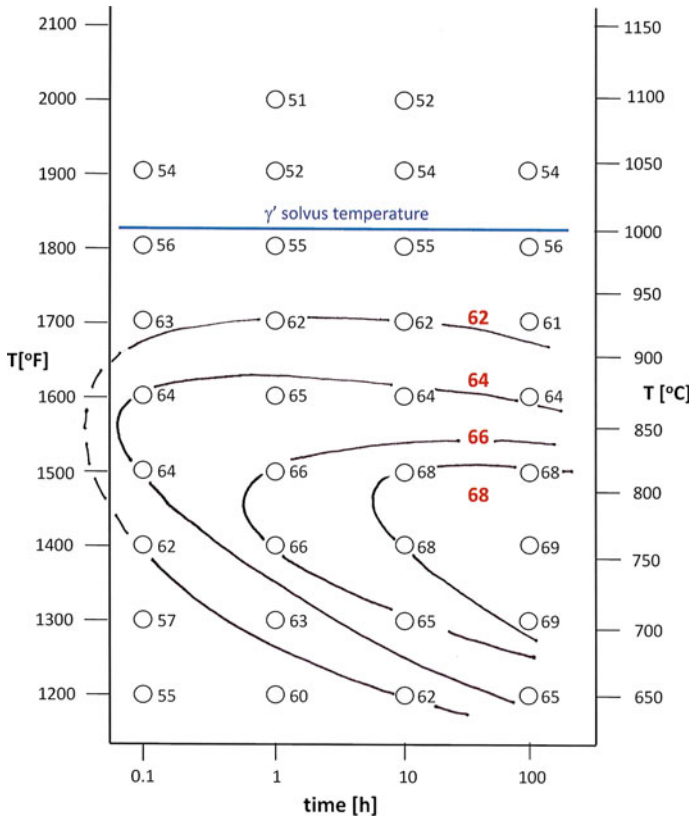
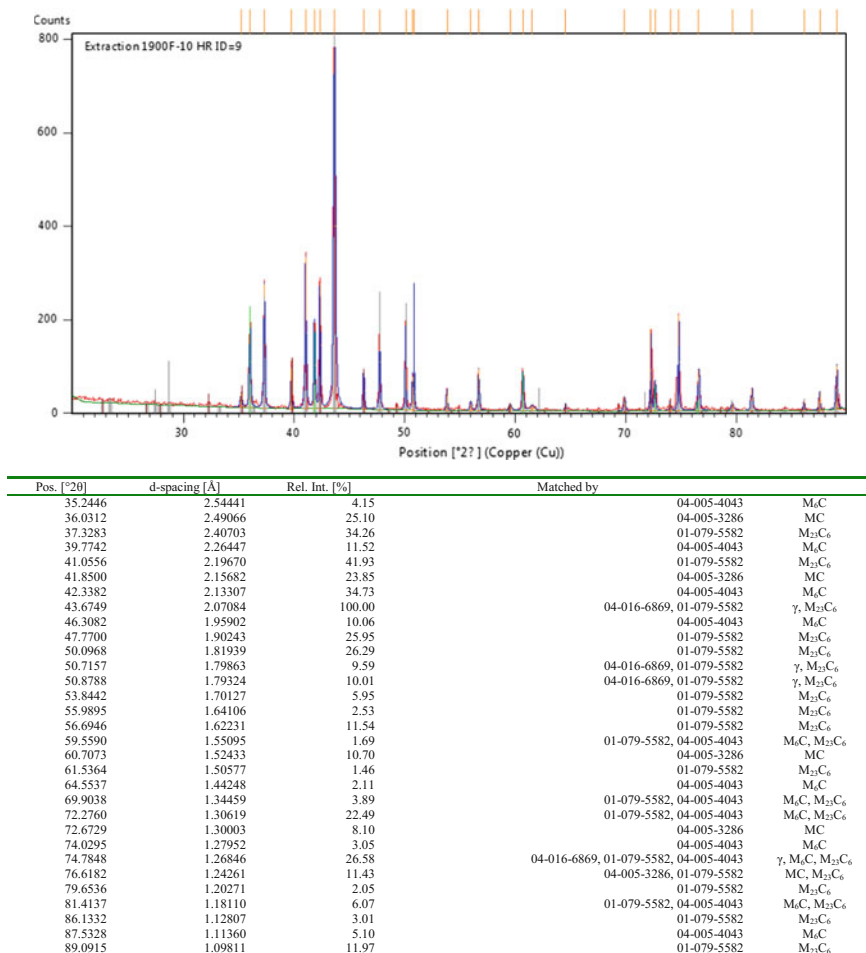


Fig. 6 Time-temperature-hardness diagram of 282 alloy. Hardness in Rockwell A. Notice that a 69 Rockwell A hardness corresponds to roughly 36 Rockwell C hardness

## Thermal Exposures—Secondary Carbides

Phase extraction/XRD work on 100-h exposed samples showed that virtually all diffraction peaks could be indexed by the  $\gamma$  matrix phase, MC-type,  $M_6C$ -type, and  $M_{23}C_6$ -type carbides as demonstrated exemplarily in Fig. 7. No additional phases



Ref. Code	Chemical Formula	Compound Name	Crystal System
04-016-6869	Cr <sub>0.32</sub> Mo <sub>0.04</sub> Co <sub>0.64</sub>	Chromium Cobalt Molybdenum	Cubic
04-005-3286	Ti <sub>0.5</sub> Mo <sub>0.5</sub> C <sub>0.83</sub>	Titanium Molybdenum Carbide	Cubic
01-079-5582	Cr <sub>23</sub> C <sub>6</sub>	Chromium Carbide	Cubic
04-005-4043	Mo <sub>3</sub> Co <sub>3</sub> C	Molybdenum Cobalt Carbide	Cubic

**Fig. 7** 2- $\theta$  diffraction scan of residue extracted from a 282 alloy sheet sample exposed 1038 °C (1900 °F)/100 h, and peak matching with powder diffraction file PDF-4+ database. Note that the compound name chromium cobalt molybdenum represent the  $\gamma$  matrix, titanium molybdenum carbide represents MC, chromium carbide represents  $M_{23}C_6$ , and molybdenum cobalt carbide represents  $M_6C$



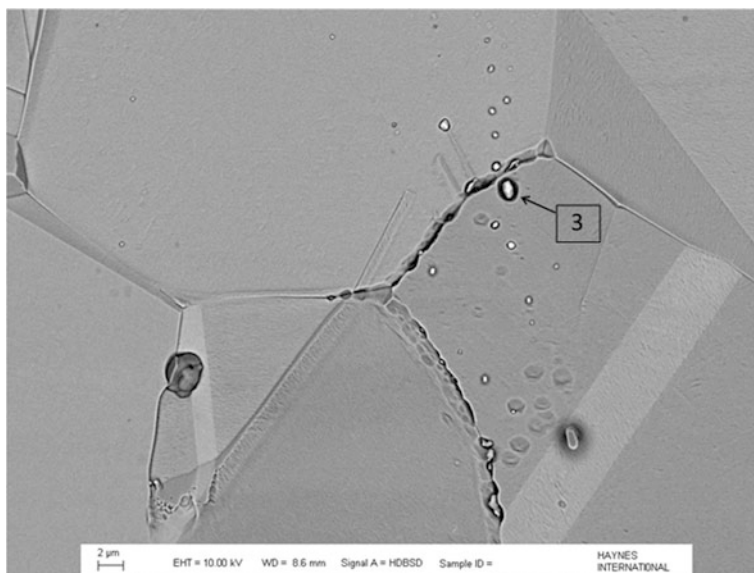


**Fig. 8** High-magnification SEM BSE photomicrograph of a 282 alloy sheet sample exposed 1121 °C (2050 °F)/6 min, exhibiting primary MC and primary  $M_6C$  carbides

were identified for the studied exposure conditions. Since MC-type and  $M_6C$ -type carbides were already found (by SEM/EDS) in the initial condition, it was concluded that the secondary carbides were chiefly  $M_{23}C_6$ -types and perhaps additional  $M_6C$ -types. The latter conjecture was addressed by detailed SEM/EDS work.

Determination whether a potential secondary carbide particle indeed formed during thermal exposure or was already present in the initial mill-annealed condition proved difficult at times as illustrated by the BSE image in Fig. 8. Compositionally, the particle with label 3 was clearly identified as  $M_6C$ . However, the fact that it did not reside in a grain boundary and that in its vicinity a string of similarly bright particles were observed in this BSE image, lead to the conclusion that this particular particle was most likely present in the mill-annealed condition. Another important criterion for distinction between primary and secondary carbides was based on the observation that the bulk of the secondary carbides formed in the grain boundaries. This is quite common in Ni-base superalloys since both types of secondary carbides feature very large unit cells [6] that are difficult to nucleate homogeneously in the bulk of the grain.

Another experimental difficulty resulted from the small size of the secondary carbides in certain exposure conditions, and the associated matrix interference in the EDS analyses. In this case, the results were inconclusive.

The outcome of the SEM/EDS compositional analyses of these secondary carbides is compiled in Tables 2 and 3. Recalling the standard-less nature of these analyses and the potential interference by the matrix, it appears that the chemical

**Table 2** Composition of secondary  $M_{23}C_6$  carbides in thermally exposed 282 alloy measured by standard-less SEM/EDS (in at.%)

Exposure temperature [°C (°F)]	Element	0.1 h exposure	1 h exposure	10 h exposure	100 h exposure
1093 (2000)	C		16.1	20.2	
	Co		–	–	
	Ni		11.4	13.8	
	Mo		10.0	9.5	
	Cr		62.5	56.5	
1038 (1900)	C		17.4	19.8	21.5
	Co		–	–	–
	Ni		22.1	15.7	9.4
	Mo		8.1	8.5	9.5
	Cr		51.3	55.2	59.5
982 (1800)	C	20.6	25.2	18.1	22.5
	Co	–	–	–	–
	Ni	23.0	16.2	14.2	9.4
	Mo	7.2	8.4	9.4	8.4
	Cr	49.2	49.1	58.3	59.7
927 (1700)	C	20.7	20.7	16.8	
	Co	–	4.7	3.9	
	Ni	27.6	23.5	17.9	
	Mo	6.9	6.7	7.5	
	Cr	42.9	42.3	52.0	
871 (1600)	C		22.5	17.1	
	Co		4.1	4.8	
	Ni		19.1	24.4	
	Mo		7.3	7.1	
	Cr		45.6	45.2	
816 (1500)	C			23.1	
	Co			–	
	Ni			24.0	
	Mo			7.1	
	Cr			44.8	

compositions of both types of secondary carbides did not vary significantly with exposure time and temperature. Moreover, in the case of  $M_6C$ , there was also very little difference between the composition of the primary and the secondary carbide particles.

The outcome of the detailed qualitative analyses of the phase constitution of the exposed samples is shown graphically in Fig. 9. Approximate C-curves were constructed for the  $M_{23}C_6$  and  $M_6C$  secondary carbides. Several conclusions can be drawn from this figure:

**Table 3** Composition of secondary M<sub>6</sub>C carbides in thermally exposed 282 alloy measured by standard-less SEM/EDS (in at.%)

Exposure temperature [°C (°F)]	Element	Primary M <sub>6</sub> C carbide	10 h exposure	100 h exposure
1093 (2000)	C	15.3	14.4	
	Co	6.9	7.1	
	Ni	26.2	25.9	
	Mo	28.9	29.6	
	Cr	18.3	19.2	
	Ti	3.1	2.7	
1038 (1900)	C		15.0	19.3
	Co		6.5	6.0
	Ni		25.1	25.6
	Mo		30.7	27.7
	Cr		18.5	16.8
	Ti		2.9	2.7
982 (1800)	C		16.6	15.5
	Co		–	7.1
	Ni		30.0	26.4
	Mo		30.3	28.8
	Cr		19.0	18.1
	Ti		2.6	3.1
927 (1700)	C		17.1	13.5
	Co		7.5	7.8
	Ni		28.5	27.7
	Mo		24.8	27.4
	Cr		20.4	18.3
	Ti		1.4	3.2
871 (1600)	C			24.5
	Co			7.3
	Ni			22.4
	Mo			27.9
	Cr			15.1
	Ti			1.9
816 (1500)	C			12.9
	Co			10.1
	Ni			24.1
	Mo			30.6
	Cr			18.9
	Ti			2.4

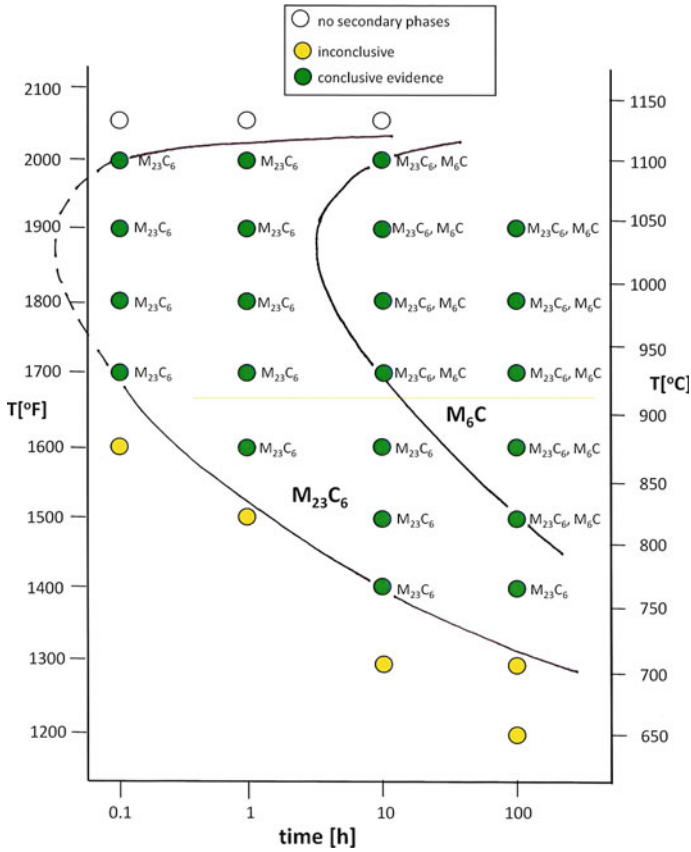


**Fig. 9** Proposed time-temperature-transformation diagram of 282 alloy with approximate C-curves for  $M_{23}C_6$  and secondary  $M_6C$  carbides

- (1) The kinetics of precipitation of  $M_{23}C_6$  carbides in the grain boundaries are approximately two orders of magnitude faster than that of the  $M_6C$  carbides.
- (2) The solvus temperatures of both secondary carbides appear to be in the vicinity of 1121 °C (2050 °F).

The former conclusion can be rationalized by the known sluggish diffusivity of Mo, the key  $M_6C$ -forming element, compared to that of Cr, the key  $M_{23}C_6$ -forming element [9]. We note that the latter conclusion is quite discrepant from several CALPHAD-type phase constitution simulations: the presence of  $M_{23}C_6$  carbides at these high temperatures is not predicted.

Secondary carbides in Ni-base superalloys can affect grain size evolution during thermo-mechanical processing, and are known to impact key mechanical properties such as creep resistance and ductility. However, it is not only their nature, but also their size and distribution in the grain boundaries that determine their impact. It is

generally accepted that discrete grain boundary carbides are beneficial to creep strength, while not unduly degrading ductility. Such discrete grain boundary decoration was observed at all exposures above the  $\gamma'$  solvus. Accordingly, the recommended two-step aging cycle of 282 alloy encompasses a first aging step at 1010 °C (1850 °F) for 2 h. Therefore, the results of this study have confirmed the implications of the standard 2-step aging treatment (1010 °C/2 h + 788 °C/8 h) for 282 alloy: the first step resulting in discrete  $M_{23}C_6$  carbides at the grain boundary, and the second step providing the optimal age-hardening.

We note that the presented results are consistent with those published previously [10] for 1,000-h exposures at similar temperatures, in that the alloy (a) forms secondary  $M_{23}C_6$  and  $M_6C$  carbides, and (b) that no additional phases were found. The latter finding warrants some discussion. At the typical boron levels in the alloy, the presence of sub-micron sized Mo-rich  $M_3B_3$  boride particles was reported by Osoba et al. [11]. However, these authors performed detailed TEM work to arrive at this conclusion. The methods employed here (SEM/EDS, phase extraction/XRD) lead only to a conclusion that the amount of any boride would have been below the detection limits. Another possibility for the lack of borides is the potential partitioning of B to a  $M_{23}(C,B)_6$  type carbide, as suggested for alloy 617B [12]. Lastly, TCP phases such as  $\mu$  and  $\sigma$  (both predicted by CALPHAD software) were not found to have formed even for extended exposure times, presumably on account of their sluggish precipitation kinetics at  $T < 816$  °C (1500 °F).

## Summary and Conclusions

1. Utilizing commercial sheet stock, an approximate TTT diagram of HAYNES 282 alloy was generated.
2. In the initial, mill-annealed condition, primary TiN, (Ti,Mo)C, a few  $M_6C$  carbides, and very fine cooling  $\gamma'$  were found to be present.
3. Upon exposure at temperatures ranging from 649 to 1093 °C (1200–2000 °F) and times up to 100 h, secondary  $M_{23}C_6$  and  $M_6C$  carbides formed in the grain boundaries. The kinetics of precipitation of secondary  $M_{23}C_6$  carbides seems to be roughly two orders of magnitude faster than that of secondary  $M_6C$  carbides, however, the solvus temperatures of both phases appear to be in the vicinity of 1121 °C (2050 °F).
4. Exposures at temperatures ranging from 649 to 982 °C (1200–1800 °F) presumably coarsened the pre-existing cooling  $\gamma'$ , and resulted in significant hardening for certain exposure conditions.
5. By SEM and XRD methods only, borides could not be detected. Deleterious TCP phases were not found for any of the studied exposure conditions.

**Acknowledgements** J. Schrader, M. A. Richeson, J. A. Ryan, B. North, and J. P. Cotner are thanked for sample preparation and detailed LM/SEM/EDS/XRD work. Helpful discussions with D. A. Metzler are acknowledged.

## References

1. Pike LM (2011) NI-CR-CO alloy for advanced gas turbine engines, Haynes International, assignee. US Patent 8,066,938, 20 Nov 2011
2. JMatPro, Sente Software Ltd. <http://www.sentesoftware.co.uk/1899.aspx>
3. TC-PRISMA, Thermo-Calc software AB. <http://www.thermocalc.com>
4. PanPrecipitation, CompuTherm LLC. <http://www.computherm.com>
5. Pike LM (2008) Development of a fabricable gamma-prime ( $\gamma'$ ) strengthened superalloy. In: Reed RC, Green KA, Caron P, Gabb TP, Fahrmann MG, Huron ES, Woodard SR (eds) Proceedings 11th international symposium on superalloys. The Minerals, Metals & Materials Society, Pittsburgh, pp 191–200
6. PDF-4+ (2016) International centre of diffraction data, Newtown Square, PA, 2016
7. Rasband WS (1997–2016) ImageJ. National Institutes of Health, Bethesda, MD. <http://imagej.nih.gov/ij>
8. Metzler DA (2017) Personal communication. Haynes International Inc., Kokomo, IN
9. Reed RC (2006) The superalloys. University Press, Cambridge, UK, p 263
10. Pike LM (2010) Long term thermal exposure of HAYNES 282 alloy. In: Ott EA, Groh JR, Banik A, Dempster I, Gabb TP, Helmink R, Liu X, Mitchell A, Sjöberg GP, Wusatowska-Sarnek A (eds) Proceedings 7th international symposium on superalloy 718 and derivatives. The Minerals, Metals & Materials Society, Pittsburgh, pp 645–660
11. Osoba LO, Ding RG, Ojo OA (2012) Improved resistance to laser weld heat affected zone microfissuring in a newly developed superalloy HAYNES 282. Metall Mater. Trans. 43A (11):4281–4295
12. Tytco D, Choi P-P, Klöwer J, Kostka A, Inden G, Raabe D (2012) Microstructural evolution of a Ni-based superalloy (617B) at 700 °C studied by electron microscopy and atom probe tomography. Acta Mater 60:1731–1740